β-Glucan training reprograms long chain fatty acid peroxidation for reactive oxygen species production in neutrophils

Shu Cui [1], Hong-Xia Zhou [1], Hui Ren [1], Yuan-Xing Zhang [2], Qin Liu [1,2], Zhuang Wang [1,2,*], Da-Hai Yang [1,2,*]

[1] State Key Laboratory of Bioreactor Engineering, Laboratory of Aquatic Animal Diseases, East China University of Science and Technology, Shanghai 200237, China

[2] Shanghai Engineering Research Center of Maricultured Animal Vaccines, Shanghai 200237, China

* Corresponding authors: zhuangwang@ecust.edu.cn (ZW), dahaiyang@ecust.edu.cn (DY)

ABSTRACT

Neutrophils exposed to certain microbial stimuli undergo metabolic reprogramming, is a critical process for initiating trained immunity; however, the underlying molecular mechanisms remain largely unknown. In this study, by establishing a β-glucan training model in turbot, we found that this training enhanced the reactive oxygen species (ROS) production and intracellular fatty acid metabolism in head kidney-derived neutrophils. Notably, the acyl-CoA oxidase 1 (ACOX1) was revealed to be significantly upregulated in trained neutrophils and contributed to ROS generation, through direct peroxidation of long-chain fatty acids. Pharmacological inhibition of the ACOX1-ROS axis markedly impaired the myeloperoxidase (MPO) activity and suppressed neutrophil extracellular traps (NETs) formation in trained neutrophils, thereby reducing bacterial clearance capacity. Based on these observations, we extended our findings to a murine model and found that β-glucan training induced a conserved phenotype in bone marrow-derived neutrophils, which exhibited increased peroxisomal ACOX1-dependent ROS generation, further supporting the conserved role of this pathway in reprogramming the function of neutrophils. Taken together, our work demonstrates that β-glucan training reprograms the intracellular ACOX1-ROS axis of neutrophils, which may contribute to better understanding the metabolic mechanisms for trained immunity, and identifies the ROS generation pathway as a potential target for modulating the function of neutrophils.

Keywords: ACOX1; Bactericidal activity; Neutrophils; Peroxidation; ROS; Trained immunity

INTRODUCTION

Trained immunity refers to the innate immune memory induced by certain microbial stimuli, including β-glucan and BCG (Mhlanga et al., 2025; Netea et al., 2011; Vuscan et al., 2024). This immune program has been identified in various innate immune cells, such as monocytes, macrophages, neutrophils, natural killer (NK) cells, and dendritic cells (DCs) (Eljaszewicz et al., 2021; Kleinnijenhuis et al., 2014; Netea & Joosten, 2024; Vuscan et al., 2025; Zhu et al., 2022). Among them, neutrophils are the most abundant circulating innate immune cells, which have emerged as key players in trained immunity (Burn et al., 2021). For instance, peripheral neutrophils display heightened expression of inflammatory cytokines after training with lipoteichoic acid (LTA) or lipopolysaccharide (LPS) (Lajqi et al., 2021, 2022). Moreover, BCG-trained neutrophils show increased IL-8 expression and ROS production upon challenge with *Candida albicans* (Moorlag et al., 2020). In addition, zymosan-trained neutrophils exhibit elevated MPO expression and enhanced bactericidal activity when challenged with *Listeria monocytogenes* (Ciarlo et al., 2020). Together, these studies suggest that neutrophils play important roles in trained immunity-mediated host defense.

Multiple metabolic pathways have been revealed to be critical for neutrophil-engaged trained immunity, including glycolysis, the pentose phosphate pathway, and fatty acid metabolism (Kalafati et al., 2023). Recently, Wang *et al.* (2023) reported that glucose-6-phosphate (G6P) levels are increased in LPS-trained granulocytes, suggesting an enhanced glycolysis in trained immunity. Moreover, the transcription of hexose-6-phosphate dehydrogenase (H6PD), 6-phosphogluconolactonase (PGLS),

fatty acid synthase (FASN), and acetyl-CoA carboxylase α (ACACA) was found to be upregulated in high-glucose-trained neutrophils (Shrestha et al., 2024), indicating that activation of the pentose phosphate pathway and fatty acid metabolism may contribute to trained immunity. In addition, metabolic signals have also been shown to play critical roles in the antibacterial functions of trained neutrophils, including enhanced phagocytosis, ROS production, and NETs formation (Das et al., 2024; Shrestha et al., 2024). Specifically, inhibiting the glycolysis pathway with 2-deoxy-D-glucose (2-DG) treatment could abolished the enhanced TNF-α and ROS production in LPS-trained granulocytes (Wang et al., 2023). Meanwhile, neutrophils differentiated from *ex vivo*-trained hematopoietic stem and progenitor cells (HSPCs) also displayed elevated mitochondrial ROS production following *C. albicans* infection (Sobén et al., 2025). These studies suggest that reprogramming of metabolic pathways is a key mediator of the antibacterial activity in trained neutrophils; however, the precise molecular mechanisms underlying ROS production remain to be clarified.

In teleost, neutrophils are revealed to be served as one of the major effector cells for trained immunity. For example, Gomes *et al.* (2023) demonstrated that sublethal *Shigella* exposure could induce a trained immunity phenotype in zebrafish neutrophils, characterized by marked enrichment of H3K4me3 modifications at the promoter regions of genes involved in microbial recognition and mitochondrial ROS production. Similarly, *Salmonella* training in zebrafish was shown to enhance neutrophil differentiation with heightened mitochondrial ROS production, thereby increasing their bactericidal capacity (Darroch et al., 2023). Moreover, in β-glucan-trained turbot model,

the head kidney-derived neutrophils were revealed to exhibit higher activation of the IL-1R and NF-κB signaling pathways, leading to enhanced lactate production, ROS generation, and NETs formation (Mu et al., 2022). These studies suggest that trained neutrophils may undergo intracellular metabolic reprogramming linked to ROS production; however, the metabolic pathways that coordinate the antibacterial activity of trained neutrophils remain largely unknown.

In this study, to clarify the metabolic pathways involved in trained neutrophils, we established a β-glucan training model in turbot and found that β-glucan training provoked heightened ROS production upon *Edwardsiella piscicida* infection. Further investigation revealed that the elevated ROS was originated from peroxisome-specific peroxidation of long-chain fatty acids (LCFAs), which were catalyzed by ACOX1, rather than from mitochondrial β-oxidation. Evolutionarily, this metabolic reprogramming-engaged ACOX1-ROS axis was found to be conserved in a murine model of trained neutrophils. Taken together, these results indicate that β-glucan training can reprogram LCFA peroxidation-dependent ROS production in both mammalian and teleost neutrophils, which may provide a promising strategy to combat bacterial infections across vertebrates.

MATERIALS AND METHODS

Experimental animals and ethics statement

Turbot (*Scophthalmus maximus*) were obtained from Tianyuan Corp. (Yantai, China) and acclimated for one week in a recirculating aquaculture system (Haisheng, China). All fish were maintained in artificial seawater at 15±2°C, with total ammonia nitrogen below 0.5 mg/L and dissolved oxygen above 5.0 mg/L. Healthy fish weighing 30±2 g were randomly selected for experiments. C57BL/6 mice (4 weeks old) were obtained from Shanghai Jiesijie Laboratory Animal (Shanghai, China) and kept under controlled temperature (22±1°C) with a 12 h light/dark cycle. The animal experiments conducted in this study were performed in accordance with the guidelines of the Animal Experiment Committee of East China University of Science and Technology (Protocol No. 2006272). All surgery was carried out under carbon dioxide anesthesia, and all efforts were made to minimize suffering.

Bacteria strain

Edwardsiella piscicida strain EIB202 (CCTCC No. M208068) was inoculated on tryptic yeast broth (TYB) and cultured overnight at 30°C. A single colony was then transferred to fresh TYB medium containing colistin (16.7 μg/mL) and grown at 30°C with shaking at 200 r/min for 12h. The culture was subsequently diluted 1:100 into fresh antibiotic-free TYB and incubated under static conditions for infection experiments.

Neutrophil isolation

Neutrophils derived from turbot head kidney or mouse bone marrow were isolated by density gradient centrifugation using Percoll reagents as previously reported (Marchi et al., 2014; Zhao et al., 2022). Briefly, the Percoll stock solution (BioDee Biotech, China) was mixed with 1.5 mol/L NaCl at a 9:1 ratio to prepare 100% Percoll isolation fluid. For turbot model, the cell suspension from head kidney was passed through a 40 μm cell strainer and then layered onto a discontinuous Percoll gradient (51%/61%, density range 1.067-1.078 g/mL). After centrifugation at 400×***g*** for 40 min at 4°C, the cell layer between the 61% and 51% Percoll fractions was collected. For mice model, bone marrow cells were passed through a 40 μm cell strainer and then layered onto a discontinuous Percoll gradient (55%/65%/75%). The cell layer between the 65% and 75% Percoll fractions (density range 1.082–1.093 g/mL) was collected after centrifugation at 1 200×***g*** for 30 min at 26°C.

Experiment model

The *in vivo* β-glucan training and *ex vivo* neutrophil challenge model was performed as previously described (Mu et al., 2022; Kalafati et al., 2020). Briefly, healthy turbot or mice were intraperitoneally injected with 100 μL of β-glucan solution (1 mg/mL) or an equivalent volume of PBS as a control. After 7 days of rest, neutrophils were isolated and seeded into 24-well plates containing Opti-MEM (Invitrogen, USA). For turbot model, the cells (1×10^7 cells/well) were challenged with *E. piscicida* at a multiplicity of infection (MOI) of 10 for 2h before subsequent experiments. For mice model, the cells (1×10^6 cells/well) were challenged with phorbol myristate acetate

(PMA) (50 nmol/L, MedChemExpress) for 2h before subsequent experiments. For inhibitor pre-treatment, isolated neutrophils were pre-incubated with the respective inhibitors for 1h prior to the secondary challenge (2-DG: 10 mmol/L, N-acetylcysteine: 20 mmol/L, C75: 50 mmol/L, perhexiline: 5 mmol/L, 10,12-tricosadiynoic acid: 0.5 mmol/L, MedChemExpress). For cytotoxicity analysis, inhibitor-treated neutrophils were incubated with propidium iodide (PI, 10 μg/mL) for 5 min, and the percentage of PI-positive cells was then analyzed by flow cytometry.

RNA extraction and RT-qPCR

At 2 hours post-infection (hpi), the cells were harvested from the 24-well plates and lysed with 1 mL of TRIzol (Invitrogen, USA). Total mRNA was extracted from turbot head kidney-derived neutrophils (n=6) using the TRIzol-chloroform method, with three parallel mRNA samples serving as biological replicates. cDNA was synthesized using the TransScript Uni All-in-One First-Strand cDNA Synthesis SuperMix for qPCR (TransGen, China). Gene expression was analyzed on a QuantStudio 3 system (Thermo Fisher, USA) using Green qPCR SuperMix (TransGen, China) under the following cycling conditions: 94°C for 30 s, followed by 40 cycles of 94°C for 10 s and 60°C for 30 s. Relative changes in gene expression were normalized and calculated using the $2^{-\Delta\Delta Ct}$ method. The primers used in this study are listed in Supplementary Table S1.

RNA-seq and data analysis

For RNA-seq, total mRNA was extracted from turbot head kidney-derived neutrophils (isolated from six turbot per group) using the TRIzol-chloroform method

after *E. piscicida* challenge, with three parallel samples serving as biological replicates. Sequencing was performed on the Illumina NovaSeq 6000 platform (PE150). Raw reads were processed with Trimmomatic for quality filtering and adapter removal. Libraries were prepared using the NEBNext Ultra™ RNA Library Prep Kit and purified with AMPure XP beads. The sequencing data (CRA040630) were processed and analyzed using the Seurat package (v.4.4.0). Differentially expressed genes (DEGs), defined as those with $|\log_2(\text{fold change})| > 1$ and P-value < 0.05, were identified using DESeq2 (v.1.38.3). Principal component analysis (PCA) was applied to genes with marked variation in expression across groups. The DEGs were further analyzed by heatmap visualization and Gene Ontology (GO) enrichment using the gseGO function, implemented in R (Conesa et al., 2016). For single-cell RNA-seq data retrieval, the raw data (GSE195628) were analyzed using Uniform Manifold Approximation and Projection (UMAP) and the FindAllMarkers function; the resulting DEGs were subjected to GO analysis using the Metascape platform (Butler et al., 2018).

ROS production assay

At 2 hpi, neutrophils were harvested from the 24-well plates and incubated with the ROS probe DCFH-DA (Beyotime, China) at 37 °C for 20 min. After washing three times with serum-free medium to remove extracellular probe, fluorescence intensity was measured at an excitation wavelength of 488 nm and an emission wavelength of 525 nm. For superoxide (O_2^-) detection, mouse neutrophils were seeded into a 96-well plate, incubated with the fluorescent probe dihydroethidium (DHE, Beyotime), and fluorescence intensity was recorded at the indicated time points (0, 0.25, 0.5, 1, 2, 3, 4,

5, and 6h). For hydrogen peroxide (H_2O_2) detection, mouse neutrophils were seeded into a 96-well plate, incubated with Amplex Red and horseradish peroxide (Beyotime, China), and absorbance at 570 nm (OD_{570}) was measured at the indicated time points (0, 0.25, 0.5, 1, 2, 3, 4, 5, and 6h).

MPO activity assay

At 2 hpi, neutrophils were harvested and lysed in 200 μL of cell lysis buffer (Beyotime, China). The supernatants were then collected and assayed using an MPO activity kit (Nanjing Jiancheng, China), with absorbance measured at 540 nm. Enzyme activity was calculated according to the manufacturer's protocol.

NETs formation assay

At 2 hpi, 1 μL of Sytox Green (0.5 mmol/L; Invitrogen, USA) was added to the cell culture supernatant and incubated at room temperature for 5 min. Neutrophil extracellular trap (NET) formation was then measured using a microplate reader at an excitation wavelength of 485 nm and an emission wavelength of 530 nm.

Bacterial colonization assay

At each indicated time point, 100 μL of the infected cell samples or head kidney tissue homogenates was collected and serially diluted in PBS to an appropriate concentration. After thorough mixing, 5 μL of each dilution was spotted onto deoxycholate hydrogen sulfide lactose (DHL, 65.2 g/L) agar plates and incubated at 30 °C for 24 h. The colonies were then enumerated to determine the bacterial load.

Fatty acid peroxidation assay

At each indicated time point, neutrophils were harvested from the 24-well plates and incubated with the probe BODIPY 581/591 C11 (Beyotime, China) at 37 °C for 30 min. After washing three times with serum-free medium to remove excess probe, the neutrophils were analyzed by flow cytometry (Beckman, USA). Following exclusion of dead cells and cell aggregates, fluorescence signals from the reduced and oxidized forms of the probe were measured at excitation/emission wavelengths of 581/591 nm and 488/510 nm, respectively. The fluorescence intensity ratio was calculated based on the signals detected at 581/591 nm and 488/510 nm using FlowJo software.

Western blot

At 2 hpi, neutrophils were lysed in RIPA buffer and boiled with protein loading buffer (Beyotime). Equal amounts of protein from each sample were separated by SDS-PAGE on 12% gels and transferred to PVDF membranes (Merck, Germany). The membranes were blocked with 5% non-fat milk in PBST overnight at 4 °C, then incubated with anti-ACOX1 antibody (1: 1 000, ABclonal, China) for 4 h at room temperature. After washing, the membranes were incubated with goat anti-mouse IgG-HRP antibody (1: 20 000, Huabio, China) for 2 h at room temperature. Protein bands were visualized using enhanced chemiluminescence (ECL) substrate (Epizyme Biotech, China) and imaged with an automated chemiluminescence imaging system (Tanon, China) with a 5-second exposure.

In vivo β-glucan training model and inhibitor treatment

Healthy turbot were intraperitoneally injected with 100 μL of β-glucan solution (1 mg/mL) or an equivalent volume of PBS as a control. After 7 days of rest, the fish were immersed in a 30 L system containing 2×10^7 CFU/mL *E. piscicida* for 10 min. The ROS production inhibitor N-acetylcysteine (NAC, 4.5 mg/fish, MedChemExpress) or the ACOX1 inhibitor 10,12-tricosadiynoic acid (TriA, 0.3 mg/fish, MedChemExpress) was administered intraperitoneally before and after *E. piscicida* immersion infection, as previously reported (Kalimeris et al., 2016; Zeng et al., 2017). At 3 and 7 dpi, the head kidneys were collected and stored at 4°C for subsequent experiments.

Histopathology analysis

Head kidney samples were collected and fixed in paraformaldehyde fixative (Servicebio, China) for 24 to 48 h. The tissues were then dehydrated through an ethanol gradient, cleared with xylene-ethanol mixtures, and embedded in paraffin (Macklin, China). For hematoxylin and eosin (H&E) staining, the samples were cut into 5 μm sections using a microtome and stained with a commercial kit (Beyotime, China) according to the manufacturer's protocol. After staining, the slides were mounted with neutral resin, air-dried, and imaged under an optical microscope (Motic, China).

Statistical analysis

Data were analyzed using GraphPad Prism v.8.0 and are presented as mean ± SD from at least three independent experiments. Statistical comparisons were performed using Student's *t*-test, one-way ANOVA, or two-way ANOVA followed by multiple

245 comparisons. Statistical significance was set at *: $p < 0.05$; **: $p < 0.01$; and ***:

246 $p < 0.001$; ns: Not significant.

247

RESULTS

β-Glucan training enhances ROS-dependent antimicrobial capacity in teleost neutrophils

To characterize the antimicrobial function of trained neutrophils in turbot, we established a β-glucan training model followed by *E. piscicida* infection (Figure 1A), and found that neutrophils derived from the head kidney of trained fish exhibited significantly increased ROS production compared to the control group at 2 hpi (Figure 1B, C). This finding was further supported by GO analysis of our previous single-cell RNA-seq data (GSE195628) (Mu et al., 2022), which showed that the biological process "response to oxidative stress" was enriched in trained neutrophils (Supplementary Figure S1; Supplementary Table S2). Meanwhile, we measured the MPO activity and NETs formation in trained neutrophils, and found that both were significantly enhanced upon *E. piscicida* challenge.

To investigate whether the ROS production is essential for regulating the antimicrobial capacity of trained neutrophils, we used the inhibitor N-acetylcysteine (NAC) (Chen et al., 2025) to scavenge ROS and assessed the above parameters. The results confirmed that this inhibitor did not affect neutrophil viability (Supplementary Figure S2). And consequently, we found that ROS scavenging significantly suppressed the enhanced MPO activity and NETs formation in trained neutrophils (Figure 1D, E). Furthermore, the augmented bacterial clearance capacity of trained neutrophils was also abolished upon ROS depletion (Figure 1F). Together, these results indicate that β-glucan training enhances the antimicrobial capacity of turbot head kidney-derived

neutrophils by upregulating intracellular ROS production, thereby functionally linking this metabolic burst to increased MPO activity and NETs formation.

β-Glucan training elevates intracellular fatty acid metabolism in neutrophils upon bacterial challenge

To uncover the mechanisms underlying the elevated ROS production in trained neutrophils, we performed RNA-seq analysis to profile the transcriptional response of trained neutrophils at 2 hpi. Principal component analysis (PCA) revealed a distinct transcriptional separation between trained neutrophils and the control group (Figure 2A). Differential gene expression analysis identified significant upregulation of fatty acid metabolism-related genes, including *elovl7a*, *cd59gpl*, and *ppt2a* (Figure 2B). GO enrichment analysis further showed significant enrichment of terms related to fatty acid derivative metabolic process, very long-chain fatty acid biosynthetic process, and acyl-CoA biosynthetic process in β-glucan-trained neutrophils (Figure 2C; Supplementary Table S3). Moreover, qPCR validation confirmed that β-glucan training enhanced the transcriptional expression of genes involved in fatty acid synthesis (*acly*, *acaca*, and *fas*), long-chain fatty acid elongation (*scd*, *fads*, and *elovl7*), and fatty acid oxidation (*cpt*) (Figure 2D, E). Meanwhile, we also assessed the glycolytic and TCA cycle pathways, which are commonly reported to be activated in trained immunity. However, the expression of glycolytic and TCA cycle rate-limiting enzymes in trained neutrophils showed no significant changes compared to the control group (Supplementary Figure S3). Taken together, these results suggest that β-glucan training may reprogram the intracellular fatty acid metabolism in turbot head kidney-derived neutrophils.

Fatty acid metabolism is essential for ROS production in trained neutrophils

To investigate whether the fatty acid metabolic reprogramming contributes to the enhanced ROS production, we pre-treated the trained neutrophils with inhibitors of fatty acid metabolism before bacterial challenge (Figure 3A, B), and confirmed that these inhibitors did not affect the viability of neutrophils (Supplementary Figure S2). Notably, treatment with the fatty acid synthesis inhibitor C75 (Rae et al., 2015) or the fatty acid oxidation inhibitor perhexiline (PE) (Ren et al., 2020) significantly suppressed the training-induced ROS burst, whereas inhibition of the glycolysis pathway with 2-DG did not (Figure 3C, D; Supplementary Figure S2). Furthermore, the β-glucan training-enhanced MPO activity and NETs formation were both reversed upon fatty acid metabolism inhibition (Figure 3E), leading to impaired *E. piscicida* clearance in trained neutrophils (Figure 3F). Taken together, these findings suggest that β-glucan training reprograms the fatty acid metabolism to drive ROS production, thereby enhancing the antibacterial activity of trained neutrophils.

ACOX1-dependent peroxisomal fatty acid oxidation fuels the ROS production in trained neutrophils

To identify the source of the elevated ROS production in trained neutrophils upon secondary infection, we stepped forward to examine the ACOX1, a peroxisomal enzyme that generates ROS via long-chain fatty acid oxidation (Teng et al., 2023), and found that the transcript levels of *acox1* were significantly upregulated in β-glucan-trained neutrophils compared to the control group. In contrast, the expression of NADPH oxidases (*nox1*, *nox4*, *nox5*, and *duox*) was not affected (Figure 4A). These

results indicate that the β-glucan training-induced increased ROS might originate from fatty acid peroxidation mediated by ACOX1, rather than from the NOX family. Consistently, trained neutrophils exhibited evidence of peroxisomal activation, with increased transcript levels of *pex11b*, *ppara*, and matrix proteins (Figure 4B; Supplementary Figure S4).

Given that ACOX1 couples ROS generation with fatty acid peroxidation, we further measured the proportion of peroxidized fatty acids and found it significantly elevated in trained neutrophils after bacterial challenge (Figure 4C). Pharmacological inhibition of ACOX1 (Zeng et al., 2017) prior to secondary infection abolished the enhanced ROS burst in trained neutrophils (Figure 4D, E). Moreover, ACOX1 blockade reversed the training-induced MPO activity and NETs formation (Figure 4F) and impaired the bacterial clearance capacity (Figure 4G). Taken together, these findings identify ACOX1-mediated peroxisomal oxidation of long-chain fatty acids as the source of heightened ROS production in β-glucan-trained neutrophils upon secondary challenge.

ACOX1-ROS axis is essential for β-glucan trained turbot against *E. piscicida* infection

To further validate the role of the ACOX1-ROS axis *in vivo*, the turbot was received intraperitoneal injections of either the ROS scavenger NAC or the ACOX1 inhibitor TriA following β-glucan training (Figure 5A). Histological analysis of the head kidney revealed that β-glucan-trained turbot maintained relatively intact renal tubule brush borders and minimal inflammatory infiltration upon *E. piscicida* challenge

(Figure 5B, C). In contrast, inhibition of either ROS or ACOX1 led to disruption of the brush border in renal tubules and inflammatory cell infiltration by 3 dpi, which worsened by 7 dpi (Figure 5B, C). Consistent with these histological findings, inhibition of ROS production or ACOX1 activity significantly impaired *E. piscicida* clearance in trained turbot (Figure 5D). Taken together, these results suggest that β-glucan training could boost antibacterial immunity in turbot by engaging the ACOX1-ROS axis *in vivo*.

Characterizing the conserved role of ACOX1-ROS axis in elevating the function of trained neutrophils in mouse model

To examine the evolutionary conservation of the mechanism identified above, we established an *in vivo* β-glucan-trained mouse model followed by *ex vivo* neutrophil stimulation (Figure 6A). Upon PMA challenge, β-glucan-trained neutrophils exhibited increased ROS production compared to the control group (Figure 6B, C), accompanied by enhanced superoxide (O_2^-) and hydrogen peroxide (H_2O_2) generation (Figure 6D). Consistent with our findings in turbot, β-glucan-trained murine neutrophils showed upregulated ACOX1 expression and enhanced intracellular fatty acid peroxidation upon restimulation (Figure 6E, F). Additionally, the *pex11b-ppara* pathway was significantly upregulated in β-glucan-trained group (Figure 6G). Furthermore, when trained neutrophils were pre-treated with an ACOX1 inhibitor before PMA challenge, the enhanced ROS production, MPO activity, and NETs formation induced by β-glucan training, were all abolished (Figure 6H). Taken together, these results suggest that β-glucan-training-induced fatty acid peroxidation in peroxisomes is conserved in both

358 teleost and murine neutrophils, leading to elevated ROS production upon secondary

359 stimulation (Figure 7).

360

DISCUSSION

In this study, our results demonstrate that β-glucan-trained neutrophils could upregulate the ACOX1-mediated fatty acid peroxidation, which functionally links ROS burst to increased MPO activity and NETs formation. Mechanistically, the lipid metabolism reprogramming is recognized as one of the core drivers for trained immunity, supplying ATP and generating immunoregulatory intermediates (Teng et al., 2023), which are revealed to originate from both exogenous uptake and *de novo* synthesis (You & Chi, 2023). For example, dietary supplementation with saturated fat has been shown to potentiate trained immunity in macrophages, enhancing their capacity to combat *C. albicans* infection (Seufert et al., 2022). Moreover, Gianfrancesco *et al.* (2019) revealed that high-fat diet-induced macrophages could promote the NLRP3 inflammasome assembly and IL-1β secretion independently of ROS and IRE-1α involvement. Thereafter, Groh *et al.* (2021) identified that oxLDL training could upregulate the fatty acid β-oxidation, providing ATP to support TNF-α expression. Additionally, recent evidences in trained granulocytes have also been revealed with heightened fatty acid synthesis in different disease models, such as sepsis and diabetes (Lavillegrand et al., 2024; Shrestha et al., 2024; Wang et al., 2023). Together with our results, these findings demonstrate that reprograming the intracellular fatty acid metabolism might be a critical issue for trained immunity, highlighting that enhanced ROS production to serve as a key mediator to shaping the function of neutrophils.

In various disease models, the enhanced intracellular ROS production represents a conserved functional hallmark of neutrophils (Alotiby, 2024; Morris et al., 2022). For example, Moorlag *et al.* (2020) observed an elevated ROS levels in BCG-trained human peripheral blood neutrophils, which correlate with enhanced clearance of exogenous bacteria. Moreover, Lajqi *et al.* (2021) revealed that LPS-trained murine neutrophils could activate the TLR4/MyD88/PI3K signaling pathway, mediating enhanced ROS production and pro-inflammatory cytokine expression upon secondary infection. Similarly, Das *et al*. (2024) identified a neutrophil subset with elevated expression of NOX family genes in the lungs of LPS-trained mice following secondary *Pseudomonas aeruginosa* infection. Consistently with our study, we observed a significant increase in fatty acid peroxidation-mediated ROS upon secondary stimulation in both teleost and murine trained neutrophils, which contribute to enhanced antibacterial capacity. However, it is worth noting that while enhanced ROS and fatty acid peroxidation are crucial for antimicrobial activity, their excessive accumulation can also trigger cell death pathways such as ferroptosis (Yang et al., 2024). Thus, whether this prolonged or repeated stimulation could tip the balance toward cell death remains to be investigated. To this end, future studies to examine the lipid peroxidation markers and cell death-related effectors (such as GPX4 and ACSL4) in trained neutrophils, would help us to delineate the boundary between beneficial antimicrobial ROS and detrimental oxidative damage.

In addition, by establishing an *in vivo* training and *ex vivo* neutrophil challenge model, our results revealed that β-glucan-trained neutrophils exhibit elevated functions

upon secondary challenge, suggesting that this process may originate from training-induced remodeling of upstream progenitors. As previously reported, the trained neutrophils are suggested to exhibit persistently elevated antimicrobial activity upon bacterial challenge, characterized by increased pro-inflammatory cytokine production, ROS generation, and NETs formation (Kalafati et al., 2023). However, the short lifespan of mature peripheral neutrophils appears inconsistent with the sustained protection conferred by trained immunity. In this regard, lineage tracing studies in mice have revealed that HSPCs exhibit trained phenotypes and display a significant bias toward myeloid cell development (de Laval et al., 2020; Liao et al., 2025). Consistently, Sobén *et al.* (2025) demonstrated that *in vitro* training of HSPCs toward neutrophil differentiation could result in significantly improved antifungal activity in mature neutrophils. Jurado *et al.* (2025) revealed that combined β-glucan and BCG training could reprogram the granulopoiesis, promoting the maturation of neutrophils with an anti-tumor phenotype. Nargis Khan *et al.* (2025) also found that β-glucan training could induce a distinct subset of immature neutrophils that confer immune tolerance and protect mice against influenza A virus. In accordance with these studies, our *in vivo* training and *in vitro* challenge model has established and revealed a conserved role of ACOX1-ROS axis in orchestrating the functional reprogramming of neutrophils. Thus, future work to investigate the development of trained progenitor cells upstream of neutrophils *in vivo* may complement the framework for better understanding the specific role of mature peripheral neutrophils in both teleost and murine models.

In summary, our study provides the evidence that β-glucan training reprograms a conserved ACOX1-dependent peroxisomal ROS axis in neutrophils of both teleost and mice. This finding uncovers the peroxisomal long-chain fatty acid peroxidation pathway as a key driver of trained neutrophils. By linking the fatty acid metabolism to ROS production, MPO activity, and NETs formation, our work establishes a mechanistic framework for understanding trained immunity in neutrophils across evolutionarily distant species. Nevertheless, several questions remain to be addressed in future studies. First, the epigenetic regulation of the *acox1* locus and the upstream signaling pathways that couple β-glucan recognition to ACOX1 upregulation await clarification. Moreover, it also remains to be determined whether ACOX1 acts as a downstream effector of general fatty acid metabolism or is governed by independent regulatory mechanisms in trained neutrophils. Second, while our murine model used PMA as a secondary stimulus, which may activate NOX2, we cannot completely rule out a contribution of NOX2-derived ROS; thus, genetic ablation of NOX2 in future experiments would help delineate the relative contributions of peroxisomal versus NADPH oxidase-derived ROS. Third, the use of perhexiline to inhibit mitochondrial fatty acid oxidation may indirectly affect substrate availability for peroxisomal peroxidation, calling for more selective genetic or pharmacological tools to dissect peroxisomal pathways. Finally, the species-specific differences in metabolic reliance between teleost and mammalian neutrophils warrant further investigation. Addressing these aspects will not only consolidate our understanding of the ACOX1-ROS axis but

446 also open new avenues for therapeutic modulation of neutrophil function in infectious

447 and inflammatory diseases.

448

DATA AVAILABILITY

The transcriptome data generated in this study were deposited in the Genome Sequence Archive (GSA) at the China National Center for Bioinformation database (https://ngdc.cncb.ac.cn/gsa; accession number GSA: CRA040630), Science Data Bank (https://www.scidb.cn; DOI: https://doi.org/10.57760/sciencedb.38752), and NCBI Sequence Read Archive (https://submit.ncbi.nlm.nih.gov/subs/sra; BioProjectID PRJNA1428719).

AUTHORS' CONTRIBUTIONS

S.C.: Investigation, Methodology, Data curation, Formal analysis, Software, Writing-original draft. **H.X.Z.**: Methodology, Data curation, Formal analysis. **H.R.**: Methodology, Data curation. **Y.X.Z.**: Writing-review & editing. **Q.L.**: Writing-review & editing. **Z.W.**: Conceptualization, Supervision, Writing-review & editing. **D.H.Y.**: Conceptualization, Supervision, Resources, Formal analysis, Project administration, Funding acquisition, Writing-review & editing. All authors read and approved the final version of the manuscript.

COMPETING INTERESTS

The authors declare that they have no competing interests.

ACKONWLEGEMENTS

This work was supported by the National Key Research and Development Program of China (No. 2022YFC2804300), the Shanghai Agriculture Innovation Program

(T2025327), the Shuguang Program of Shanghai Education Development Foundation and Shanghai Municipal Education Commission (24SG31) and the Fundamental Research Funds for the Central Universities (222201251732)

.

REFERENCES

Alotiby A. 2024. Immunology of stress: A review article. *Journal of Clinical Medicine*, **13**(21): 6394.

Burn GL, Foti A, Marsman G, et al. 2021.The neutrophil. *Immunity*, **54**(7): 1377–1391.

Butler A, Hoffman P, Smibert P, et al. 2018. Integrating single-cell transcriptomic data across different conditions, technologies, and species. *Nature Biotechnology*, **36**(5): 411–420.

Chen DY, Guo ZY, Yao L, et al. 2025. Targeting oxidative stress-mediated regulated cell death as a vulnerability in cancer. *Redox Biology*, **84**: 103686.

Ciarlo, E., Heinonen, T., Théroude, C, et al. 2020. Trained immunity confers broad-spectrum protection against bacterial infections. *The Journal of Infectious Diseases*, **222**(11): 1869–1881.

Conesa A, Madrigal P, Tarazona S, et al. 2016. A survey of best practices for RNA-seq data analysis. *Genome Biology*, **17**(1): 13.

Darroch H, Keerthisinghe P, Sung YJ, et al. 2023.Infection-experienced HSPCs protect against infections by generating neutrophils with enhanced mitochondrial bactericidal activity. *Science Advances*, **9**(26): eadf9904.

Das S, Kaminski TW, Schlegel BT, et al. 2024. Neutrophils and galectin-3 defend mice from lethal bacterial infection and humans from acute respiratory failure. *Nature Communications*, **15**(1): 4724.

de Laval B, Maurizio J, Kandalla PK, et al. 2020. C/EBPβ-dependent epigenetic memory induces trained immunity in hematopoietic stem cells. *Cell Stem Cell*, **26**(5): 657–674.

Eljaszewicz A, Ruchti F, Radzikowska U, et al. 2021. Trained immunity and tolerance in innate lymphoid cells, monocytes, and dendritic cells during allergen-specific immunotherapy. *Journal of Allergy and Clinical Immunology*, **147**(5): 1865–1877.

Gianfrancesco MA, Dehairs J, L'homme L, et al. 2019. Saturated fatty acids induce NLRP3 activation in human macrophages through K^+ efflux resulting from phospholipid saturation and Na, K-ATPase disruption. *Biochimica et Biophysica Acta (BBA)-Molecular and Cell Biology of Lipids*, **1864**(7): 1017–1030.

Gomes MC, Brokatzky D, Bielecka MK, et al. 2023. *Shigella* induces epigenetic

reprogramming of zebrafish neutrophils. *Science Advances*, **9**(11): eadf9706.

Groh LA, Ferreira AV, Helder L, et al. 2021. oxLDL-induced trained immunity is dependent on mitochondrial metabolic reprogramming. *Immunometabolism*, **3**(3): e210025.

Jurado LF, Daman AW, Li Z, et al. 2025. A fungal-derived adjuvant amplifies the antitumoral potency of Bacillus Calmette-Guérin via reprogramming granulopoiesis. *Immunity*, **58**(9): 1984–2001.

Kalafati L, Hatzioannou A, Hajishengallis G, et al. 2023. The role of neutrophils in trained immunity. *Immunological Reviews*, **314**(1): 142–157.

Kalafati L, Kourtzelis I, Schulte-Schrepping J, et al. 2020. Innate immune training of granulopoiesis promotes anti-tumor activity. *Cell*. **183**(3): 771–785.

Khan N, Tran KA, Chevre R, et al. 2025. β-Glucan reprograms neutrophils to promote disease tolerance against influenza A virus. *Nature Immunology*, **26**(2): 174–187.

Kleinnijenhuis J, Quintin J, Preijers F, et al. 2014. BCG-induced trained immunity in NK cells: Role for non-specific protection to infection. *Clinical Immunology*, **155**(2): 213–219.

Kalimeris K, Briassoulis P, Ntzouvani A, et al. 2016. N-acetylcysteine ameliorates liver injury in a rat model of intestinal ischemia reperfusion. *Journal of Surgical Research*, **206**(2): 263–272.

Lajqi T, Braun M, Kranig S, et al. 2021. LPS induces opposing memory-like inflammatory responses in mouse bone marrow neutrophils. *International Journal of Molecular Sciences*, **22**(18): 9803.

Lajqi T, Frommhold D, Braun M, et al. 2022. Gram-positive *Staphylococcus aureus* LTA promotes distinct memory-like effects in murine bone marrow neutrophils. *Cellular Immunology*, **376**: 104535.

Lavillegrand JR, Al-Rifai R, Thietart S, et al. 2024. Alternating high-fat diet enhances atherosclerosis by neutrophil reprogramming. *Nature*, **634**(8033): 447–456.

Liao WN, Zai XD, Zhang J, et al. 2025. Hematopoietic stem cell state and fate in trained immunity. *Cell Communication and Signaling*, **23**(1): 182.

Marchi LF, Sesti-Costa R, Chedraoui-Silva S, et al. 2014. Comparison of four methods for the isolation of murine blood neutrophils with respect to the release of reactive oxygen and nitrogen species and the expression of immunological receptors. *Comparative Clinical*

Pathology, **23**(5): 1469–1476.

Mhlanga MM, Fanucchi S, Ozturk M, et al. 2025. Cellular and molecular mechanisms of innate memory responses. *Annual Review of Immunology*, **43**(1): 615–640.

Moorlag SJCFM, Rodriguez-Rosales YA, Gillard J, et al. 2020. BCG vaccination induces long-term functional reprogramming of human neutrophils. *Cell Reports*, **33**(7): 108387.

Morris G, Gevezova M, Sarafian V, et al. 2022. Redox regulation of the immune response. *Cellular & Molecular Immunology*, **19**(10): 1079–1101.

Mu D, Yang J, Jiang Y, et al. 2022. Single-cell transcriptomic analysis reveals neutrophil as orchestrator during β-glucan-induced trained immunity in a teleost fish. *Journal of Immunology*, **209**(2): 783–795.

Netea MG, Joosten LAB. 2024. Trained innate immunity: Concept, nomenclature, and future perspectives. *Journal of Allergy and Clinical Immunology*, **154**(5): 1079–1084.

Netea MG, Quintin J, van der Meer JWM. 2011. Trained immunity: A memory for innate host defense. *Cell Host & Microbe*, **9**(5): 355–361.

Rae C, Haberkorn U, Babich JW, et al. 2015. Inhibition of fatty acid synthase sensitizes prostate cancer cells to radiotherapy. *Radiation Research*, **184**(5): 482–493.

Ren Z, Chen S, Seo JE, et al. 2020. Mitochondrial dysfunction and apoptosis underlie the hepatotoxicity of perhexiline. *Toxicology in Vitro*, **69**: 104987.

Seufert AL, Hickman JW, Traxler SK, et al. 2022. Enriched dietary saturated fatty acids induce trained immunity via ceramide production that enhances severity of endotoxemia and clearance of infection. *eLife*, **11**: e76744.

Shrestha S, Lee YB, Lee H, et al. 2024. Diabetes primes neutrophils for neutrophil extracellular trap formation through trained immunity. *Research*, **7**: 0365.

Sobén M, Guerrero P, Guiu A, et al. 2025. *Candida albicans*-stimulated hematopoietic stem and progenitor cells generate trained neutrophils with enhanced mitochondrial ROS production that defend against infection. *PLoS Pathogens*, **21**(4): e1013170.

Teng YJ, Xu LC, Li WJ, et al. 2023. Targeting reactive oxygen species and fat acid oxidation for the modulation of tumor-associated macrophages: a narrative review. *Frontiers in Immunology*, **14**: 1224443.

Vuscan P, Kischkel B, Joosten LAB, et al. 2024. Trained immunity: General and emerging

562 concepts. *Immunological Reviews*, **323**(1): 164–185.
563 Vuscan P, Kischkel B, Joosten LAB, et al. 2025. Microbial-induced trained immunity for
564 cancer immunotherapy. *Pharmacological Reviews*, **77**(2): 100074.
565 Wang BB, Zhu LL, Jia B, et al. 2023. Sepsis induces non-classic innate immune memory in
566 granulocytes. *Cell Reports*, **42**(10): 113044.
567 Yang X, Wang Z, Samovich SN, et al. 2024. PHLDA2-mediated phosphatidic acid
568 peroxidation triggers a distinct ferroptotic response during tumor suppression. *Cell*
569 *Metabolism*, **36**(4): 762–777.
570 You ZY, Chi HB. 2023. Lipid metabolism in dendritic cell biology. *Immunological Reviews*,
571 **317**(1): 137–151.
572 Zeng J, Deng SW, Wang YP, et al. 2017. Specific inhibition of acyl-CoA oxidase-1 by an
573 acetylenic acid improves hepatic lipid and reactive oxygen species (ROS) metabolism in
574 rats fed a high fat diet. *Journal of Biological Chemistry*, **292**(9): 3800–3809.
575 Zhao JJ, Chen WJ, Zhang YX, et al. 2022. Bacterial infection induces pyroptotic signaling-
576 mediated neutrophil extracellular traps (NETs) formation in turbot (*Scophthalmus*
577 *maximus*). *Fish & Shellfish Immunology*, **127**: 982–990.
578 Zhu WT, Su JG. 2022. Immune functions of phagocytic blood cells in teleost. *Reviews in*
579 *Aquaculture*, **14**: 630–646.
580

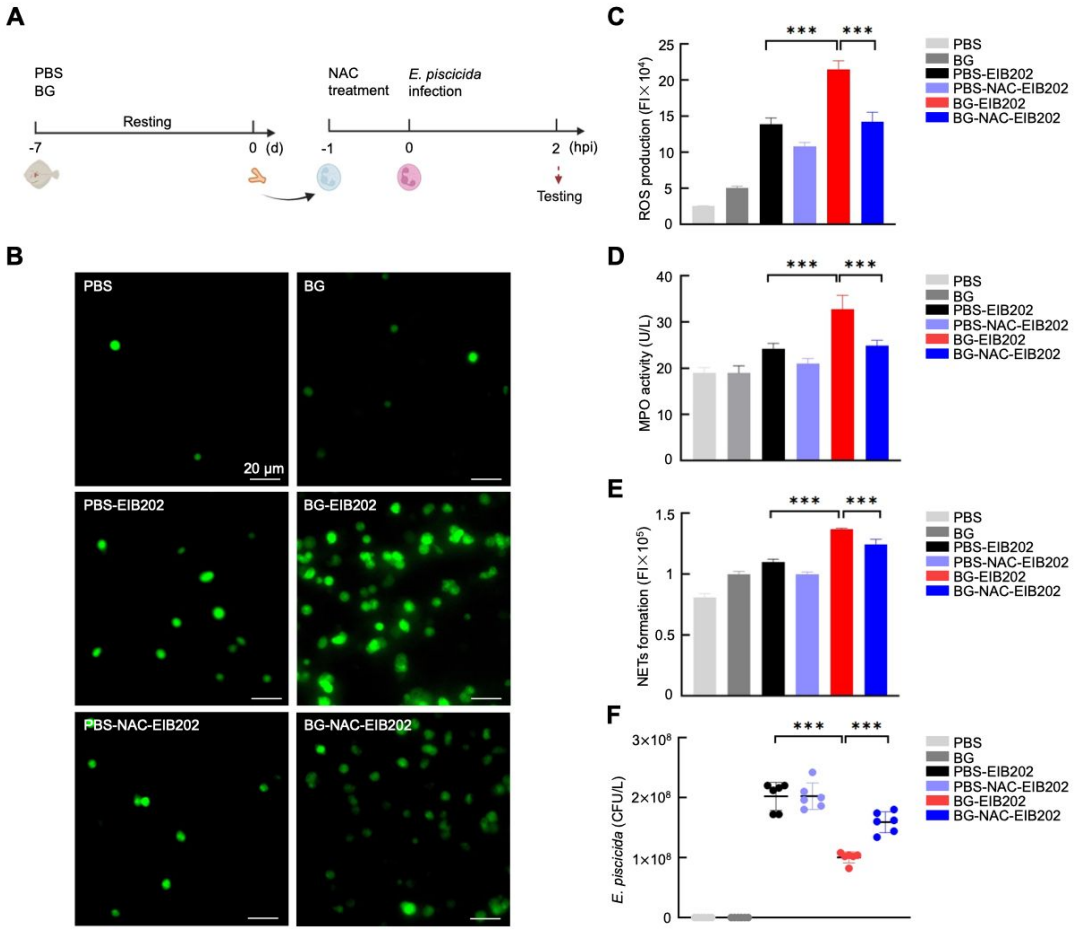

581

582 **Figure 1 β-Glucan training enhances ROS-dependent antimicrobial capacity in**

583 **turbot head kidney-derived neutrophils.** A: Schematic illustration of *in vivo* turbot

584 training and *in vitro* neutrophils challenge model with or without NAC pre-treatment.

585 B: Representative images of ROS in PBS- or β-glucan-trained neutrophils after

586 bacterial challenge, with or without NAC pre-treatment. Scale bar, 20 μm. C:

587 Quantification of ROS fluorescence intensity as indicated in panel B. D: MPO activity

588 in PBS- or β-glucan-trained neutrophils after bacterial challenge, with or without NAC

589 pre-treatment. E: NETs formation analysis (Sytox Green fluorescence intensity) in

590 PBS- or β-glucan-trained neutrophils after bacterial challenge, with or without NAC

591 pre-treatment. F: Bacterial loads analysis in PBS- or β-glucan-trained neutrophils after

bacterial challenge, with or without NAC pre-treatment. Data are from three independent experiments and presented as mean ± SD, analyzed by one-way ANOVA with multiple comparisons. ***: $P < 0.001$.

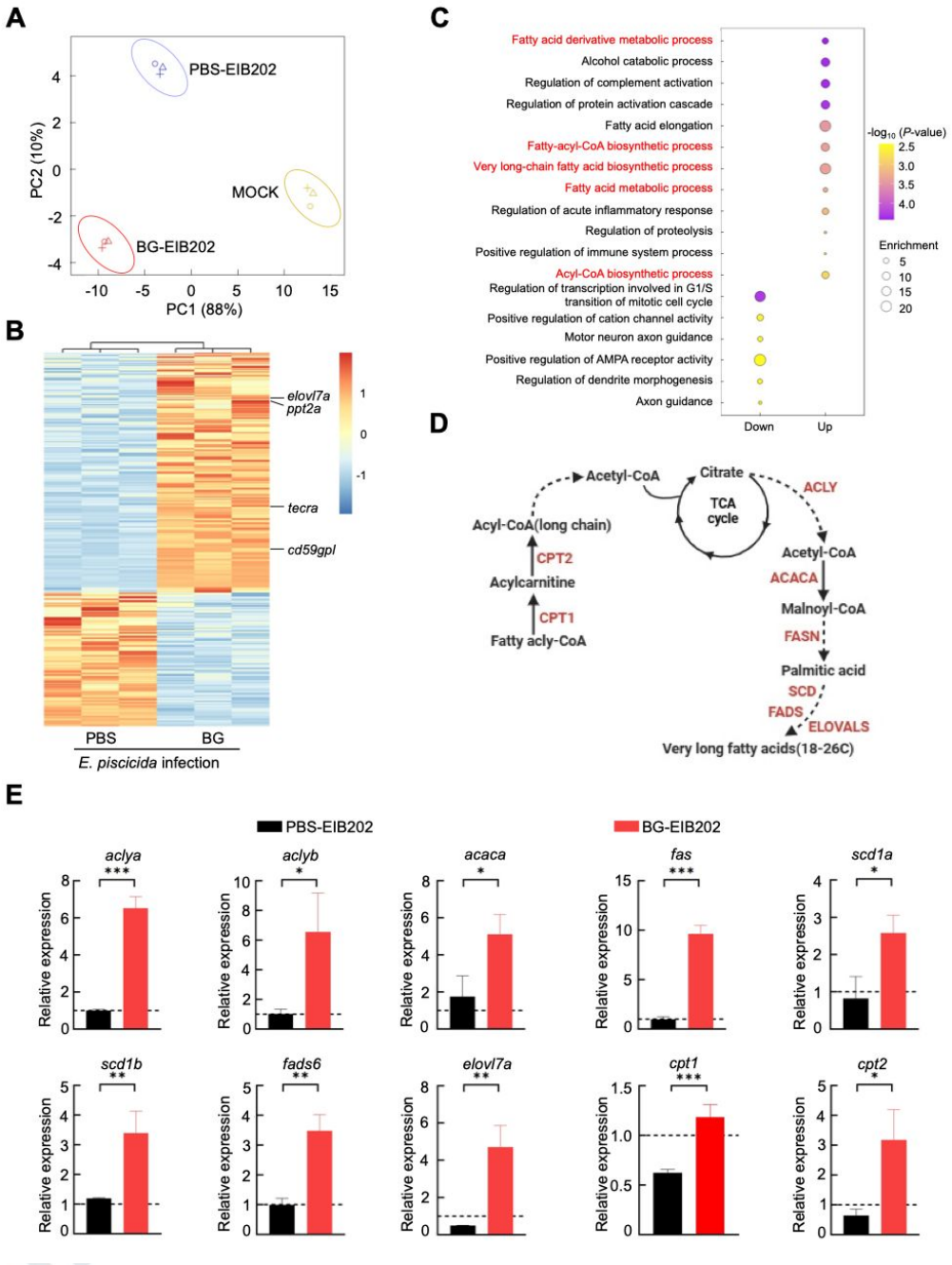

596

597 **Figure 2 β-Glucan training upregulates intracellular fatty acid metabolism in**

598 **neutrophils upon bacterial challenge**. A: Principal component analysis (PCA) of gene

599 expression in PBS- or β-glucan-trained neutrophils after bacterial challenge. B:

600 Differentially expressed genes (DEGs) between PBS- and β-glucan-trained neutrophils

601 after bacterial challenge. C: Pathway enrichment analysis of DEGs in β-glucan-trained

neutrophils compared to PBS controls. Dot size indicates the enrichment of each pathway; dot color reflects the significance level. D: Schematic diagram of fatty acid metabolism pathways in PBS- or β-glucan-trained neutrophils after bacterial challenge. E: qPCR validation of fatty acid metabolism-related gene expression in PBS- or β-glucan-trained neutrophils after bacterial challenge. Data are from three independent experiments and presented as mean ± SD, analyzed by Student's *t*-test. *: $P < 0.05$; **: $P < 0.01$; ***: $P < 0.001$.

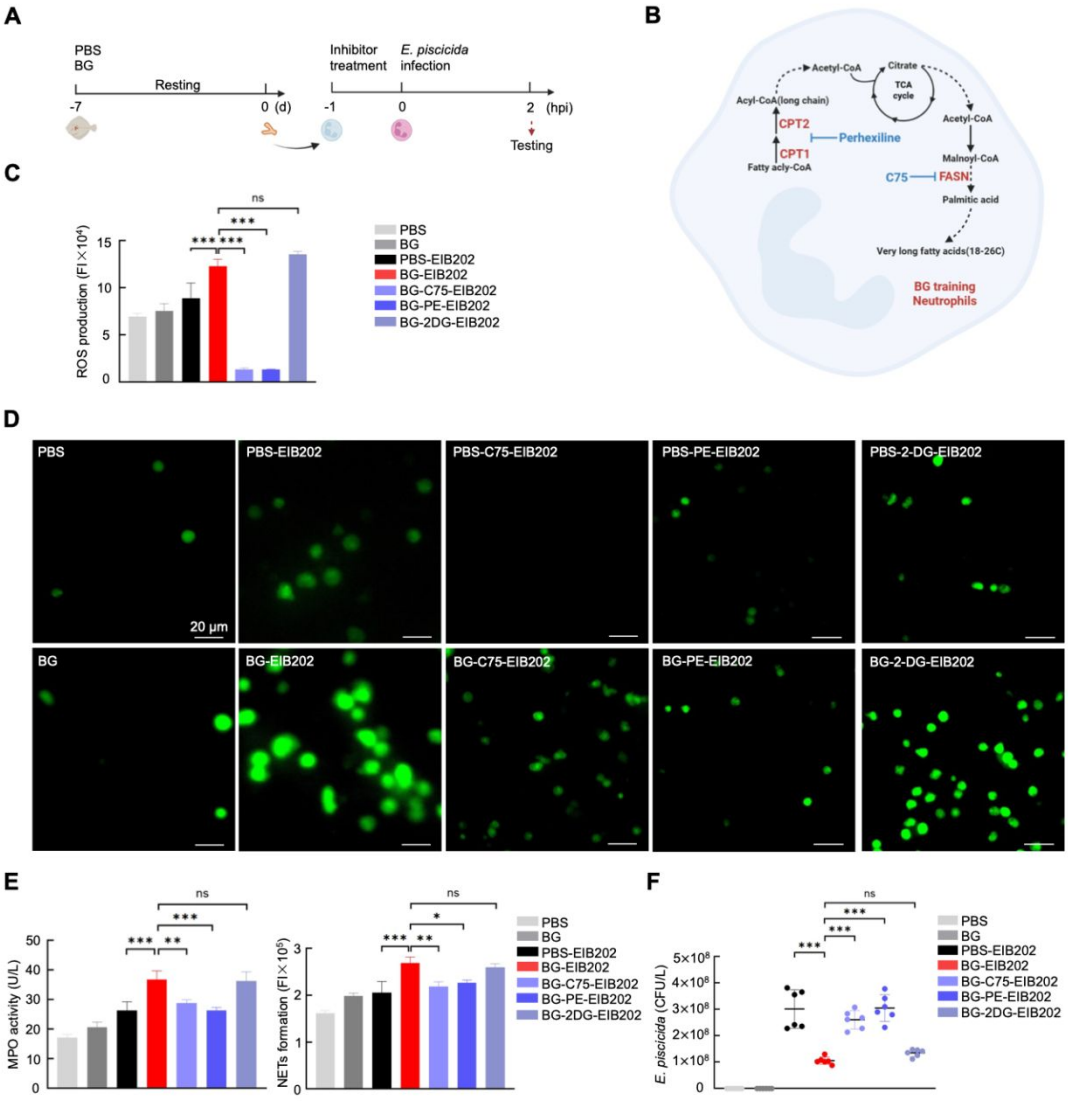

611

612 **Figure 3 Reprogramming of fatty acid metabolism is essential for ROS production**

613 **in trained neutrophils**. A: Schematic illustration of *in vivo* turbot training and *in vitro*

614 neutrophils challenge model with or without inhibitor pre-treatment. B: Diagram

615 showing the targets of inhibitors in the fatty acid metabolism pathway. C:

616 Quantification of ROS fluorescence intensity in trained neutrophils after bacterial

617 challenge, with or without inhibitor pre-treatment. D: Representative images of ROS

618 production corresponding to panel C. Scale bar, 20 μm. E: MPO activity and NETs

619 formation in trained neutrophils after bacterial challenge, with or without inhibitor pre-

620 treatment. F: Bacterial loads analysis in trained neutrophils after *E. piscicida* challenge,
621 with or without inhibitor pre-treatment. Data are from three independent experiments
622 and presented as mean ± SD, analyzed by one-way ANOVA with multiple comparisons.
623 ns: Not significant; *: $P < 0.05$; **: $P < 0.01$; ***: $P < 0.001$.

624

625

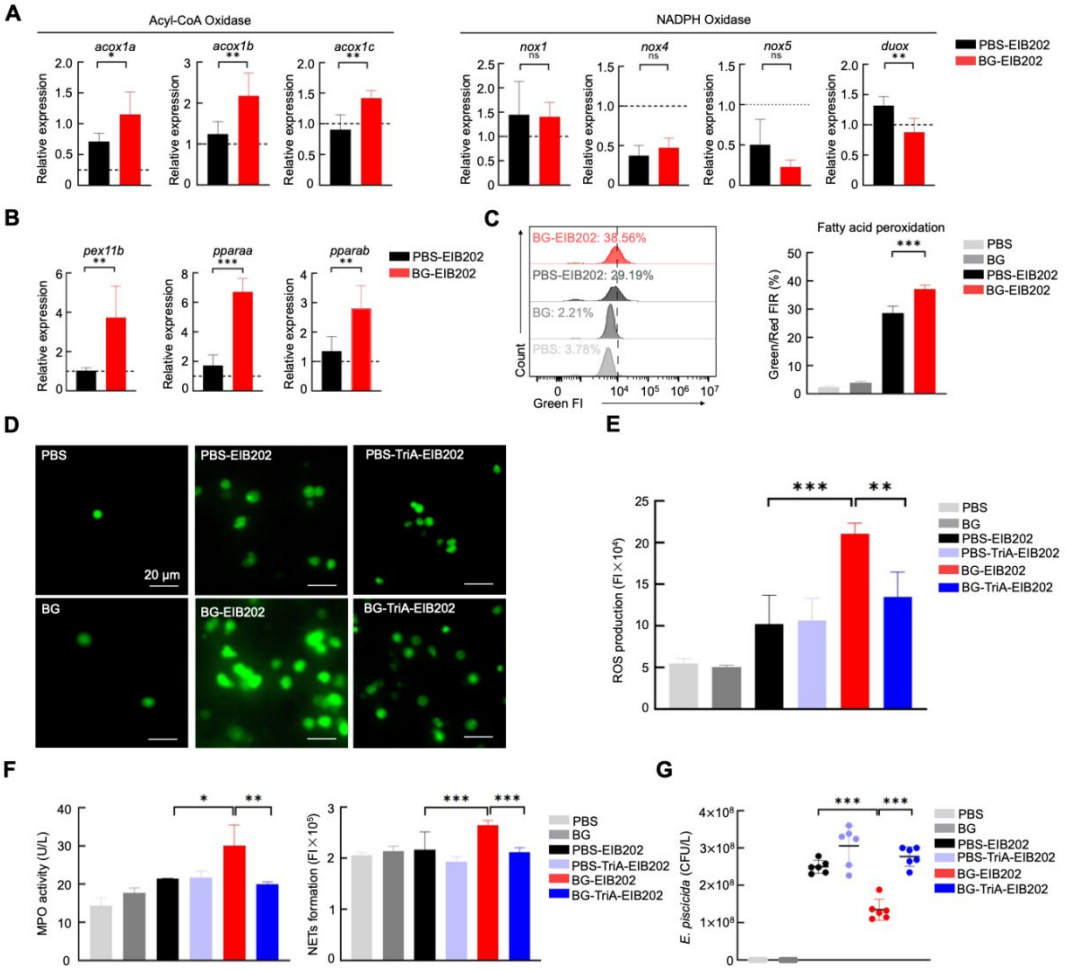

626

627 **Figure 4 ACOX1-dependent peroxisomal fatty acid oxidation fuels the ROS**
628 **increase in trained neutrophils**. A: qPCR analysis of *acox1* and NADPH oxidase
629 (*nox1, nox4, nox5, duox*) gene expression in PBS- or β-glucan-trained neutrophils after
630 bacterial challenge. B: qPCR analysis of *pex11b* and *ppara* expression in PBS- or β-
631 glucan-trained neutrophils after bacterial challenge. C: Fatty acid peroxidation levels in
632 PBS- or β-glucan-trained neutrophils after bacterial challenge. D: Representative
633 images of ROS in PBS- or β-glucan-trained neutrophils after bacterial challenge, with
634 or without TriA pre-treatment. Scale bar, 20 μm. E: Quantification of ROS fluorescence
635 intensity from panel D. F: MPO activity and NET formation in PBS- or β-

glucan-trained neutrophils after bacterial challenge, with or without TriA pre-treatment. G: Bacterial loads analysis in PBS- or β-glucan-trained neutrophils after *E. piscicida* challenge, with or without TriA pre-treatment. TriA, 10,12-tricosadiynoic acid. Data are from three independent experiments and presented as mean ± SD, analyzed by Student's *t*-test or one-way ANOVA with multiple comparisons as appropriate. ns: Not significant; *: $P < 0.05$; **: $P < 0.01$; ***: $P < 0.001$.

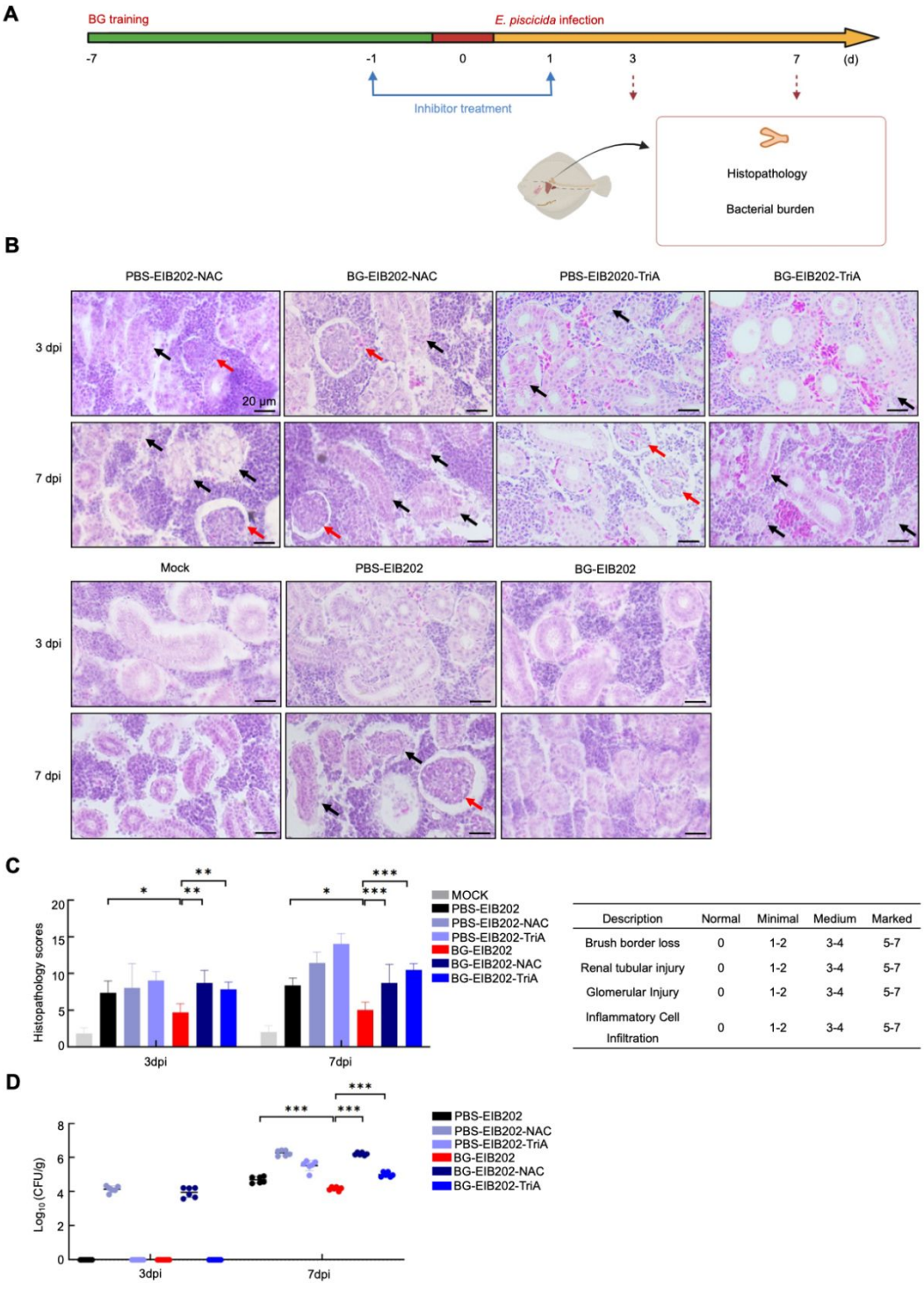

Description	Normal	Minimal	Medium	Marked
Brush border loss	0	1-2	3-4	5-7
Renal tubular injury	0	1-2	3-4	5-7
Glomerular Injury	0	1-2	3-4	5-7
Inflammatory Cell Infiltration	0	1-2	3-4	5-7

644

645 **Figure 5 β-Glucan-training-induced ACOX1-ROS axis is essential for bacterial**
646 **clearance *in vivo***. A: Schematic illustration of NAC or TriA administration during *E.*
647 *piscicida* infection in β-glucan-trained turbot. B: Histopathological analysis of head
648 kidney sections from PBS- and β-glucan-trained turbot during *E. piscicida* infection,

with or without inhibitor pre-treatment. Black arrows indicate renal tubule damage; red arrows indicate glomerulus damage. Scale bar, 20 μm. C: Histopathological scoring based on the analysis shown in panel B. D: Bacterial loads in the head kidney of PBS- or β-glucan-trained turbot during *E. piscicida* infection. with or without inhibitor pre-treatment. Data are from three independent experiments and presented as mean ± SD, analyzed by two-way ANOVA with multiple comparisons. *: $P < 0.05$; **: $P < 0.01$; ***: $P < 0.001$.

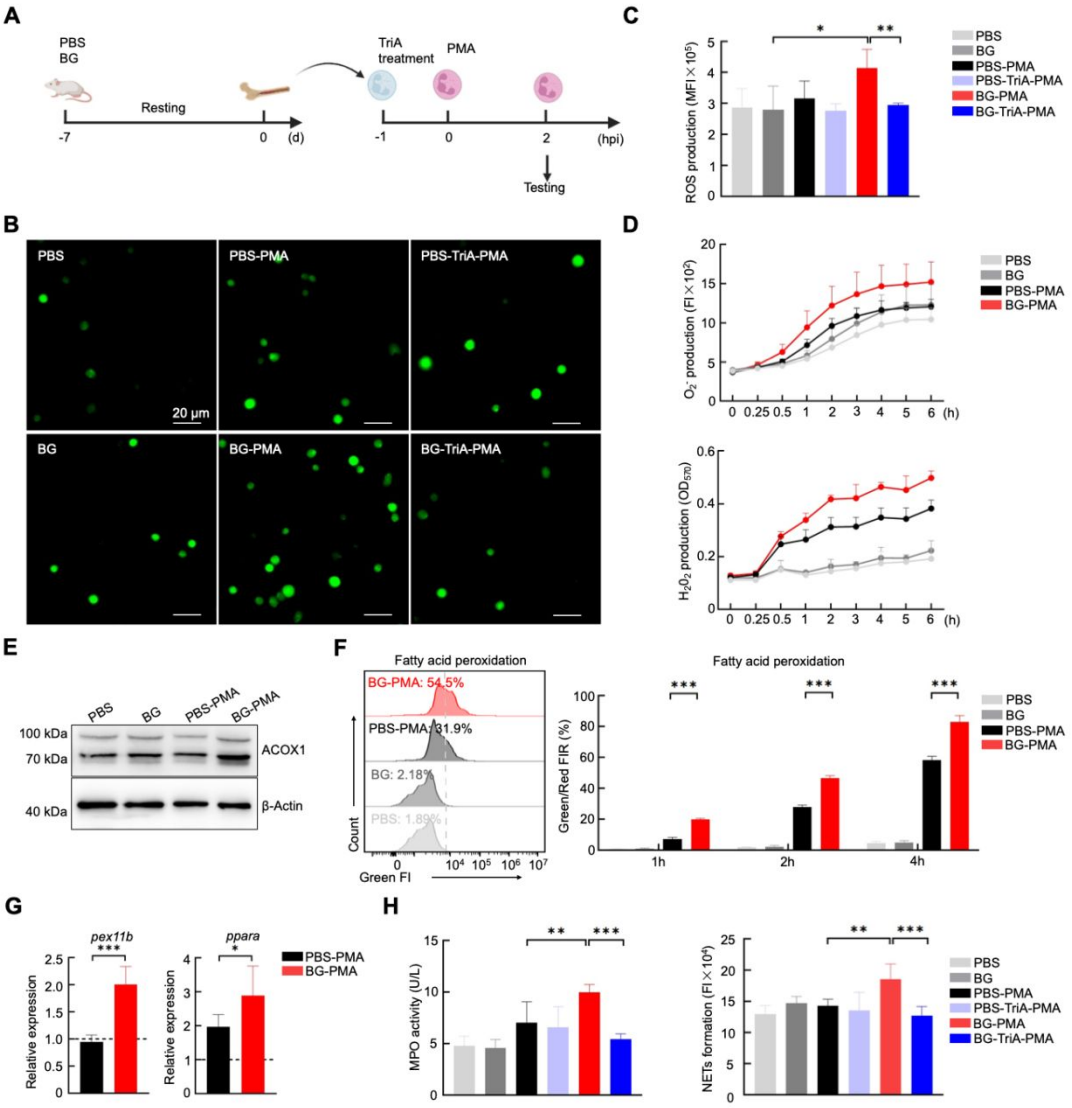

658

659 **Figure 6 β-Glucan-training-reprogrammed ACOX1-ROS axis elevates the**
660 **function of neutrophils in mouse model**. A: Schematic illustration of *in vivo* mouse
661 training and *in vitro* neutrophil challenge model with or without TriA pre-treatment. B:
662 Representative images of ROS in PBS- or β-glucan-trained neutrophils after PMA
663 challenge, with or without TriA pre-treatment. Scale bar, 20 μm. C: Quantification of
664 mean fluorescence intensity of ROS as indicated in panel B. D: Superoxide (O_2^-)
665 production and hydrogen peroxide (H_2O_2) levels (OD_{570}) in PBS- or β-glucan-trained
666 neutrophils after PMA challenge. E: Western blot analysis of ACOX1 protein

667 expression in PBS- or β-glucan-trained neutrophils after PMA challenge. F: Fatty acid
668 peroxidation levels in PBS- or β-glucan-trained neutrophils. G: qPCR analysis of
669 *pex11b* and *ppara* expression in PBS- or β-glucan-trained neutrophils after PMA
670 challenge. H: MPO activity and NETs formation analysis in PBS- or β-glucan-trained
671 neutrophils after PMA challenge, with or without TriA pre-treatment. Data are from
672 three independent experiments and presented as mean ± SD, analyzed by Student's *t*-
673 test or one-way ANOVA with multiple comparisons as appropriate. *: $P < 0.05$; **: P
674 < 0.01; ***: $P < 0.001$.

675

676

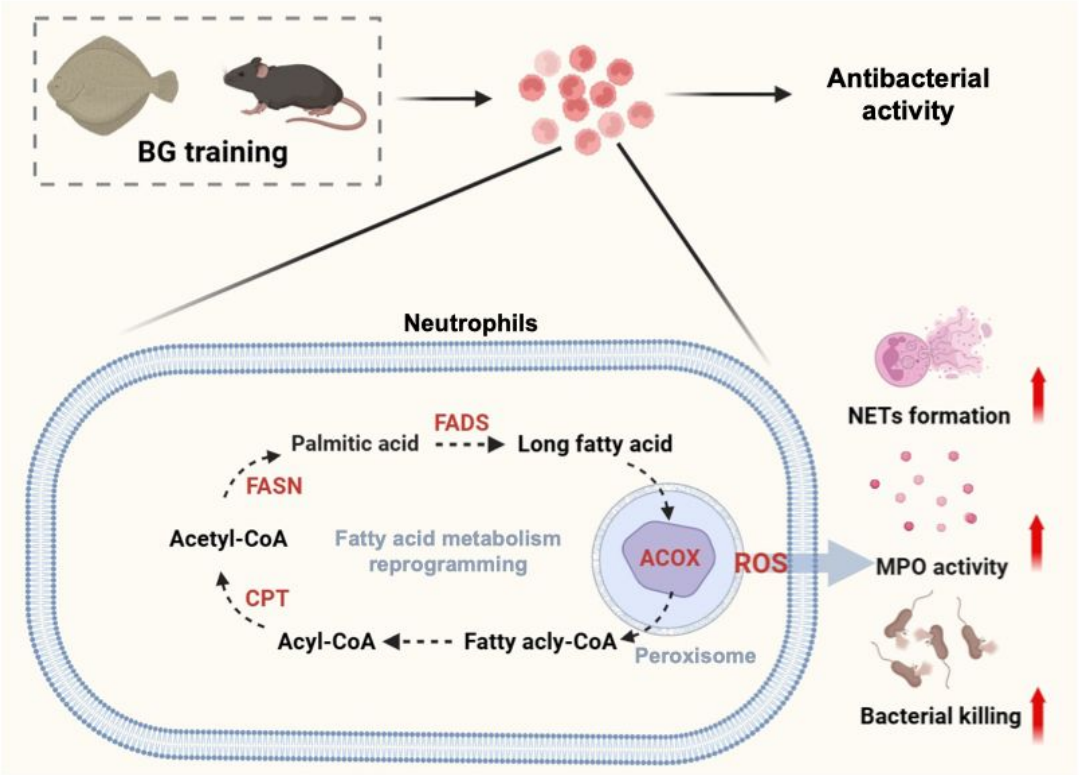

677

678 **Figure 7 Proposed mechanism of β-glucan-induced trained neutrophils via**

679 **ACOX1-ROS axis.**

680

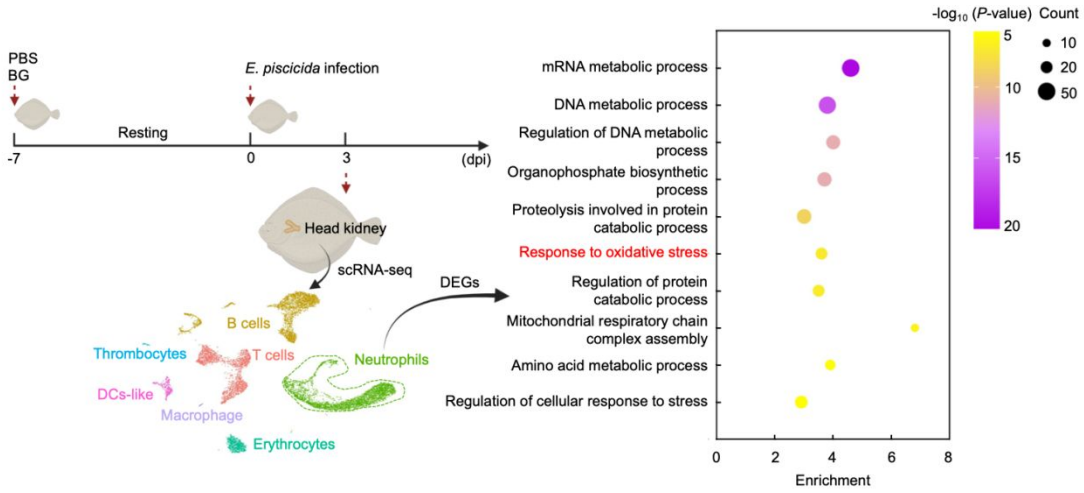

681

682 **Supplementary Figure S1. Single-cell transcriptomic analysis of the turbot head**
683 **kidney-derived neutrophils.** Landscape of immune cell clusters in turbot head kidney
684 and GO analysis of metabolism relative terms using top 50 up-regulated biological
685 process pathway in PBS- and β-glucan-trained neutrophils from single-cell RNA-seq
686 data (GSE195628). Dot size shows genes of each pathway; Dot color reflects the
687 significance of each pathway.

688

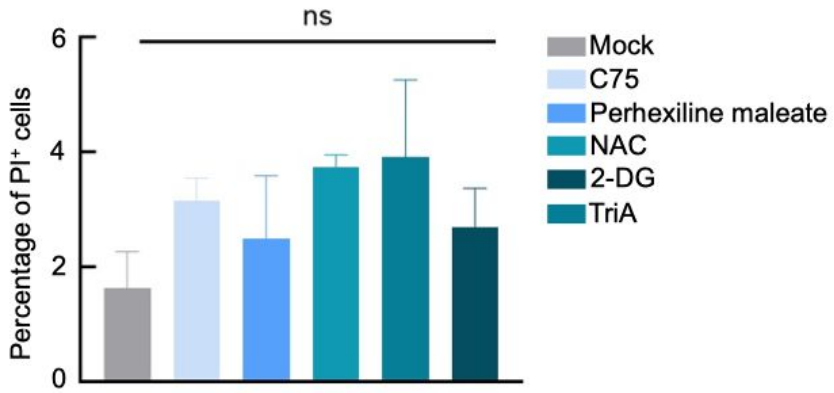

689

690 **Supplementary Figure S2. Effect of metabolic inhibitor treatment on neutrophil**

691 **viability.** Viability of turbot head kidney-derived neutrophils with inhibitors treatment

692 assessed by PI staining. Data are from three independent replicate experiments and

693 shown as mean ± SD, analyzed by one-way ANOVA with multiple comparisons. ns:

694 Not significant.

695

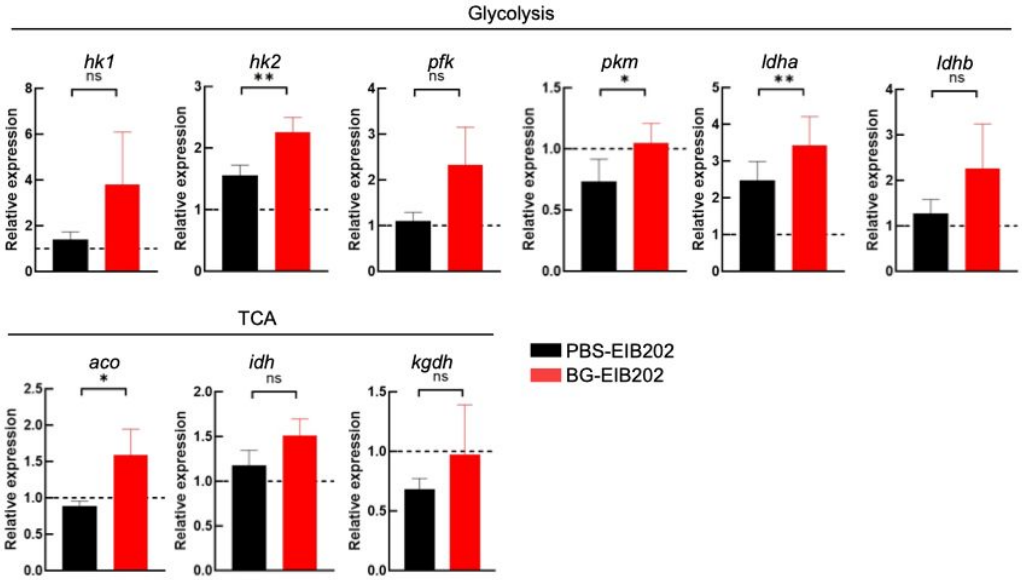

Supplementary Figure S3. mRNA levels of glycolysis and TCA cycle encoded genes in trained neutrophils. The transcripts of glycolysis and TCA cycle in PBS- and β-glucan-trained neutrophils after bacterial challenge by qPCR. Data are from three independent replicate experiments and shown as mean ± SD, analyzed by Student's *t*-test. ns: Not significant; *: $P < 0.05$; **: $P < 0.01$.

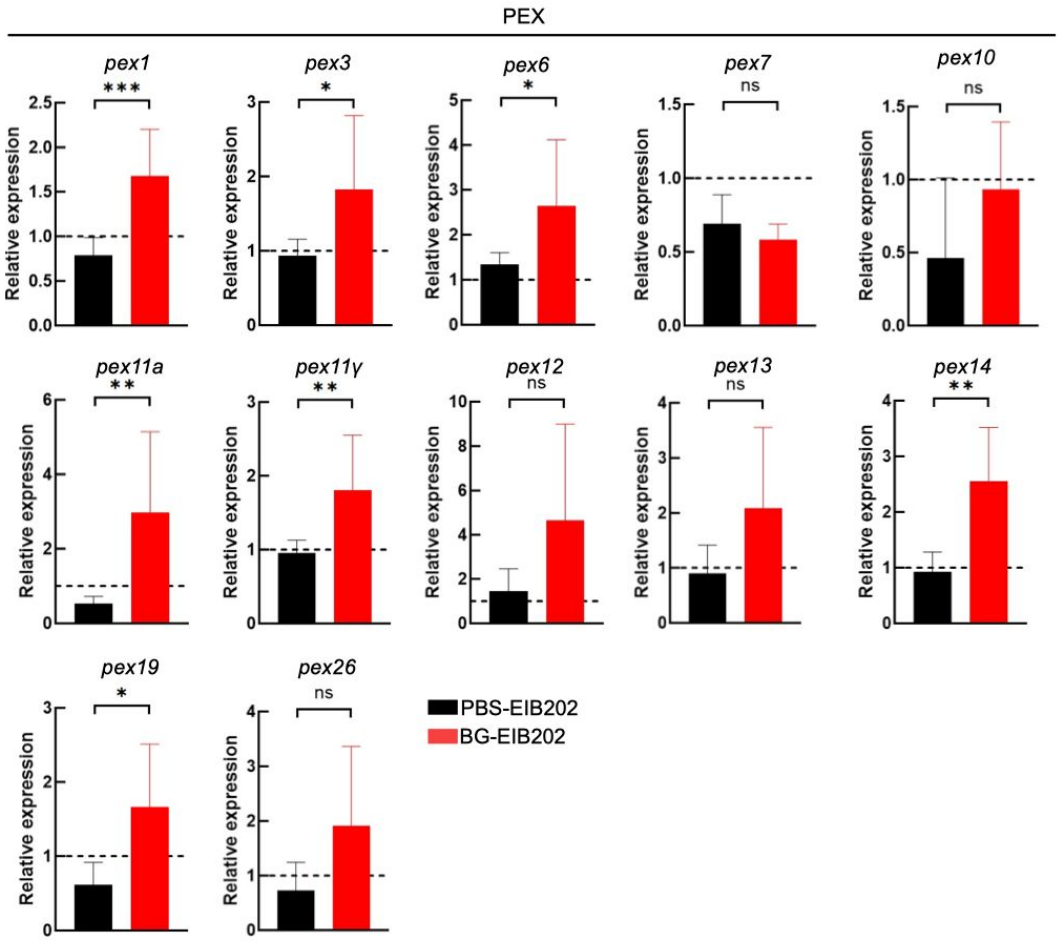

Supplementary Figure S4. mRNA levels of PEX family-encoded gene in trained neutrophils. The transcripts of PEX family-encoded genes in PBS- and β-glucan-trained neutrophils after bacterial challenge by qPCR. Data are from three independent replicate experiments and shown as mean ± SD, analyzed by Student's *t*-test. ns: Not significant; *: $P < 0.05$; **: $P < 0.01$; *** $P < 0.001$.

Supplementary Table S1. qPCR primers used in this study.

Supplementary Table S2. GO enrichment analysis of DEGs in PBS- and β-glucan -trained neutrophils after bacterial challenge.

Supplementary Table S3. GO enrichment analysis of upregulated DEGs from scRNA-seq.